

Positional information-based morphogenesis of surfactant droplet swarms emerging from competition between local and global Marangoni effects.

Pieter J. de Visser, Mink Neeleman, Pim F. J. Dankloff, Max T. G. M. Derks & Peter A. Korevaar*

Institute for Molecules and Materials, Radboud University, Heyendaalseweg 135, Nijmegen 6525 AJ, The Netherlands

Email: p.korevaar@science.ru.nl

Abstract: Positional information is proposed as a key element in morphogenesis, where cells differentiate based on their position in an external morphogen gradient. Here, we demonstrate the position-dependent differentiation of floating surfactant droplets as they self-organize in a pH gradient, using the Marangoni effect to translate gradients of surface-active molecules into motion. We start with a field of surfactant microliter-droplets floating on water, that upon the release of surfactant drive local, outbound Marangoni flows and myelin filament growth. Next, we introduce a competing surfactant based on a hydrolysable amide, which is more surface active than the myelin surfactant and thereby inhibits the local Marangoni flows and myelin growth from the droplets. Upon introducing a pH gradient, the amide surfactant hydrolyses in the acidic region, so that the local Marangoni flows and myelin growth are reestablished. The resulting combination of local and global surface tension gradients produces a region of myelin-growing droplets and a region where myelin-growth is suppressed, separated by a wave front of closely packed droplets – featuring an organization that is reminiscent to the ‘French flag’-patterns emerging from concentration gradients in morphogenesis.

Keywords: Marangoni effect, Chemical gradients, Self-organization, Amphiphiles, Adaptive behavior

1. Introduction

Designing strategies that transform molecular systems into organization of matter at the mesoscale allows for autonomous behavior emerging from the bottom-up.^[1,2] Drawing inspiration from the behavior of living organisms, such as the formation of optimized networks in slime molds to efficiently distribute nutrients,^[3,4] or the collective migration of social amoebae to survive in hostile environments,^[5-7] or the spontaneous formation of cell-like compartments from cytoplasmic components,^[8] new classes of adaptive materials can be designed with the potential to function autonomously.^[9-11] At the same time, *de novo*-designed material systems based on a minimalistic set of molecular building blocks allow us to unravel what physicochemical principles and feedback mechanisms are required for self-organization. One essential principle is the presence of spatiotemporal chemical gradients, leading to persistent anisotropy in the system.^[12,13] These gradients must be sustained actively to avoid thermodynamic equilibrium, i.e. to avoid a collapse into an isotropic, unorganized phase. Moreover, to translate chemical gradients into self-organization at the meso- or macroscale, (supra)molecular building blocks responsive to these chemical gradients are required.

The Marangoni effect provides an effective mechanism to transform concentration gradients into motion of meso- and macroscale objects, driving the organization of such objects. Starting off with concentration gradients of surface active molecules at air-liquid interfaces, the Marangoni effect leads to interfacial flow.^[14,15] When exposed to an external concentration gradient, floating objects move from low toward high surface tension regions, following the Marangoni flow (**Figure 1a**).^[16,17] Thereby, global surface tension gradients result in a localized accumulation in the high surface tension region. Introducing particles or droplets that release amphiphilic molecules extends the complexity of the self-

organization by generating local concentration gradients around the building blocks (Figure 1b). The resulting local Marangoni flows result into mutual repulsion amongst the particles, driving their organization into spread-out patterns.^[18] When combined with elastocapillary attractive effects, dynamic droplet clusters can be produced, that are typically both motile and continuously assemble and disassemble.^[19–21]

Hence, a remaining challenge is to control the positioning of self-organizing patterns based on Marangoni flows, as an alternative to either local accumulation or mutually repulsive spreading of particles. Inspired by Wolpert's concept of positional information processing – that is: cellular pattern formation based on the cells' position in an external (morphogen) concentration gradient^[22,23] – we imagined droplets in a global surface tension gradient that “interpret” the local surface tension and “differentiate” by adapting their collective positioning and morphology correspondingly. In this way, the droplets autonomously generate differently populated regions in space along the surface tension gradient, analogous to synthetic ‘French flag’-patterns that have been reported based on reaction-diffusion systems.^[24,25]

Here, we present floating surfactant droplets that autonomously produce ‘French flag’-patterns when exposed to a pH gradient. These droplets self-organize due to the competition between global and local Marangoni flows at an air-water interface (Figure 1e). Upon release of surfactant **1**, the droplets generate persistent local Marangoni flows as evidenced by the emergence of filaments, known as myelins, that have a thickness of approx. 20-50 micrometer and are extruded from the droplets into millimeter-long structures.^[26,27] A second pH-sensitive surfactant that is more surface-active than the myelin-producing surfactant inhibits the local Marangoni flow and thereby suppresses the myelin formation. When exposed to a pH gradient, the pH-sensitive surfactant is hydrolyzed in the acidic region, leading to localized reactivation of the local Marangoni flow and corresponding myelin growth. We show that for large swarms of surfactant droplets under a pH gradient, the droplets' positioning as well as their differentiation into particular morphologies is governed by the interplay of the global and local Marangoni flows. Initially, the hydrolysis of the pH-sensitive surfactant generates a global Marangoni flow towards the acidic side of the pH gradient. Subsequently, the surfactant droplets in the acidic regions start to grow myelins and generate repulsive Marangoni flows – pushing neighboring droplets away from the acidic region. Together, the competition between these local repulsive interactions and the global, attractive Marangoni flow leads to the emergence of a self-organized ‘French flag’-pattern along the pH gradient. Going from low to high pH, we observe subsequent regions of sparse – dense – sparse droplet populations, as well as a decrease of the myelin corona size. Finally, we demonstrate that the sizes of these regions are determined by the amount of acid added to the solution.

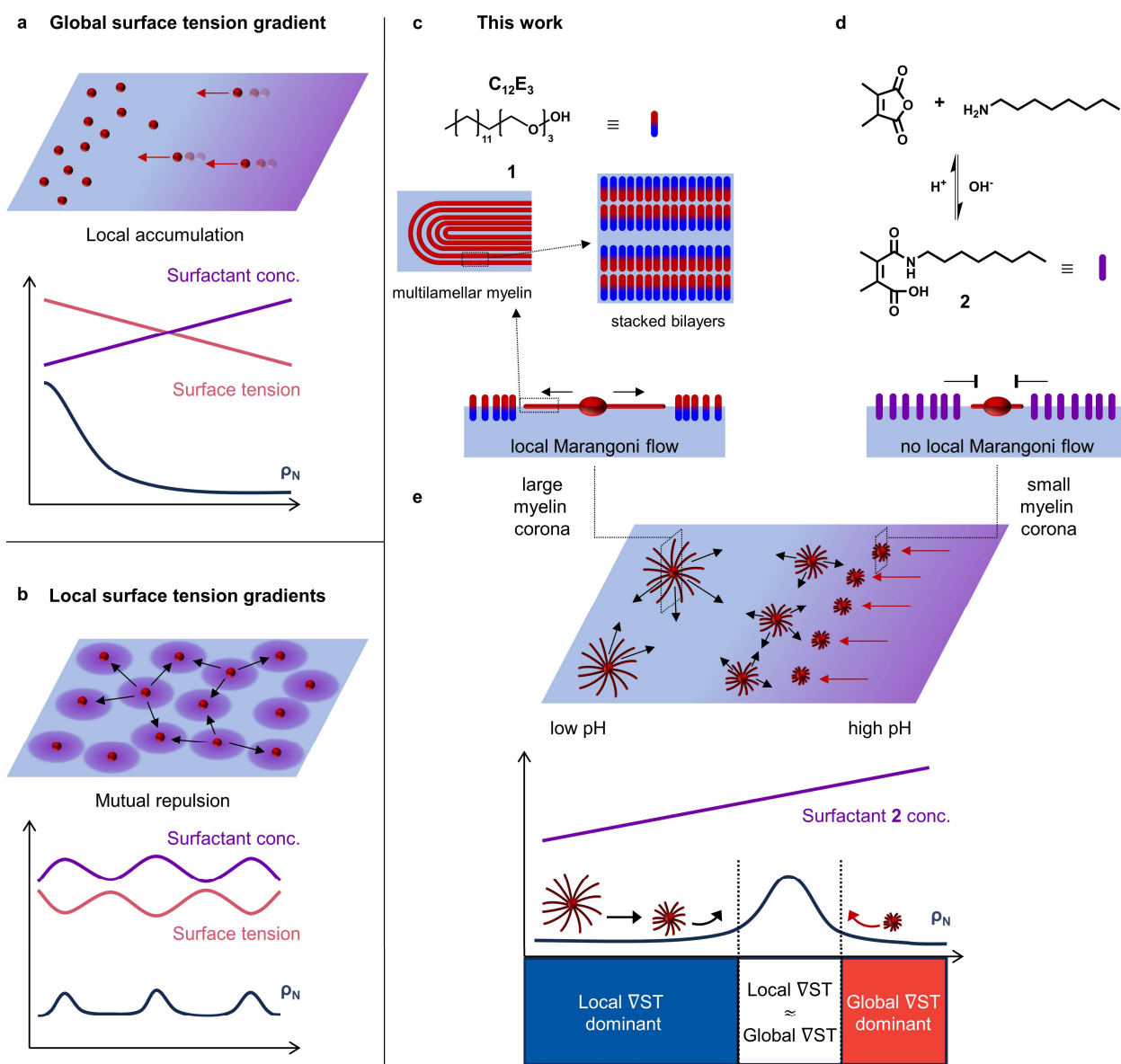


Figure 1. Self-organization of floating droplets driven by the Marangoni effect. a) Under a global surface tension gradient, Marangoni flow transports floating droplets to the region of high surface tension where they accumulate, leading to a locally high droplet density (ρ_N). b) Floating droplets that release surfactants generate local, outward Marangoni flows, leading to mutual repulsion such that the droplets spread out. c-d) In our system, two amphiphiles competitively adsorb to the air-water interface: the nonionic surfactant $C_{12}E_3$ (1) and the pH-sensitive surfactant amide 2. c) $C_{12}E_3$ droplets spontaneously form multilamellar myelin filaments when deposited at the air-water interface. $C_{12}E_3$ molecules that are released from such droplets lead to local Marangoni flows that extrude these myelins from the droplet. d) Amide surfactant 2 is formed from 1-octylamine and 2,3-dimethylmaleic anhydride (DMMA) and inhibits the local Marangoni flow generated by $C_{12}E_3$, thereby inhibiting the myelin growth. e) When a solution of amide surfactant 2 is exposed to a pH gradient, a global surface tension gradient arises, leading to a Marangoni flow towards the region of low amide surfactant 2 concentration (low pH). Subsequently, in the low pH region, $C_{12}E_3$ droplets start to generate local Marangoni flows that oppose the global Marangoni flow, whereas $C_{12}E_3$ droplets in the basic region are still inhibited by amide surfactant 2. As a result, a ‘French flag’-pattern appears of subsequent low-high-low droplet density ρ_N , determined by the balance between global and local surface tension gradients.

2. Results and Discussion

2.1. Interfacial competition between C₁₂E₃ and amide surfactant 2

As amphiphile building block for the floating droplets, we selected the nonionic amphiphile triethylene glycol monododecyl ether (C₁₂E₃, **1**). Earlier, we reported that when deposited at an air-water interface, droplets of C₁₂E₃ absorb water and concomitantly form a ‘corona’ of radially spreading filaments known as myelins,^[28,29] as shown in Figure 1c. These myelins are extruded from the droplet by the outbound Marangoni flow, which is driven by slow release of C₁₂E₃ from the droplet to the air-water interface. We determined the associated surface tension for an aqueous C₁₂E₃ solution (500 μM, approx. 10x cmc^[30]) at 27.9 ± 0.1 mN m⁻¹. Hence, to inhibit the Marangoni flow generated by the release of C₁₂E₃, the surface tension of the competing dynamic surfactant adsorbed at the air-water interface should be ≤ 27.9 mN m⁻¹.

The competing amide surfactant **2** is created in situ in an aqueous solution from 1-octylamine and 2,3-dimethylmaleic anhydride (DMMA), as reported by Liu et al. (Figure 1d).^[31] We assessed the potential of amide surfactant **2** to inhibit myelin growth by measuring the surface tension of solutions with varying concentrations of the precursors 1-octylamine and DMMA in a sodium phosphate buffer (PB, 100 mM) at pH 7. As shown in **Figure 2a**, 1-octylamine is surface active, although insufficiently to decrease the surface tension below 27.9 mN m⁻¹, i.e. to compete with C₁₂E₃. Upon increasing the concentration of DMMA added to 1-octylamine solutions, the surface tensions were observed to decrease. As DMMA is not surface active (**Figure S1**), we ascribe this decrease to the surface activity of **2** that is formed. Gratifyingly, the formation of **2** is confirmed by ¹H-NMR (**Figure S2**). Furthermore, at 1-octylamine concentrations ≥ 20 mM and DMMA concentrations ≥ 10 mM, surface tensions below the value of C₁₂E₃ were obtained. As shown in Figure 2b, the surface tension of 1-octylamine (20 mM) is approx. 37 mN m⁻¹, and decreases upon increasing the DMMA concentration to the point where it matches the surface tension of C₁₂E₃, at 7.5 mM.

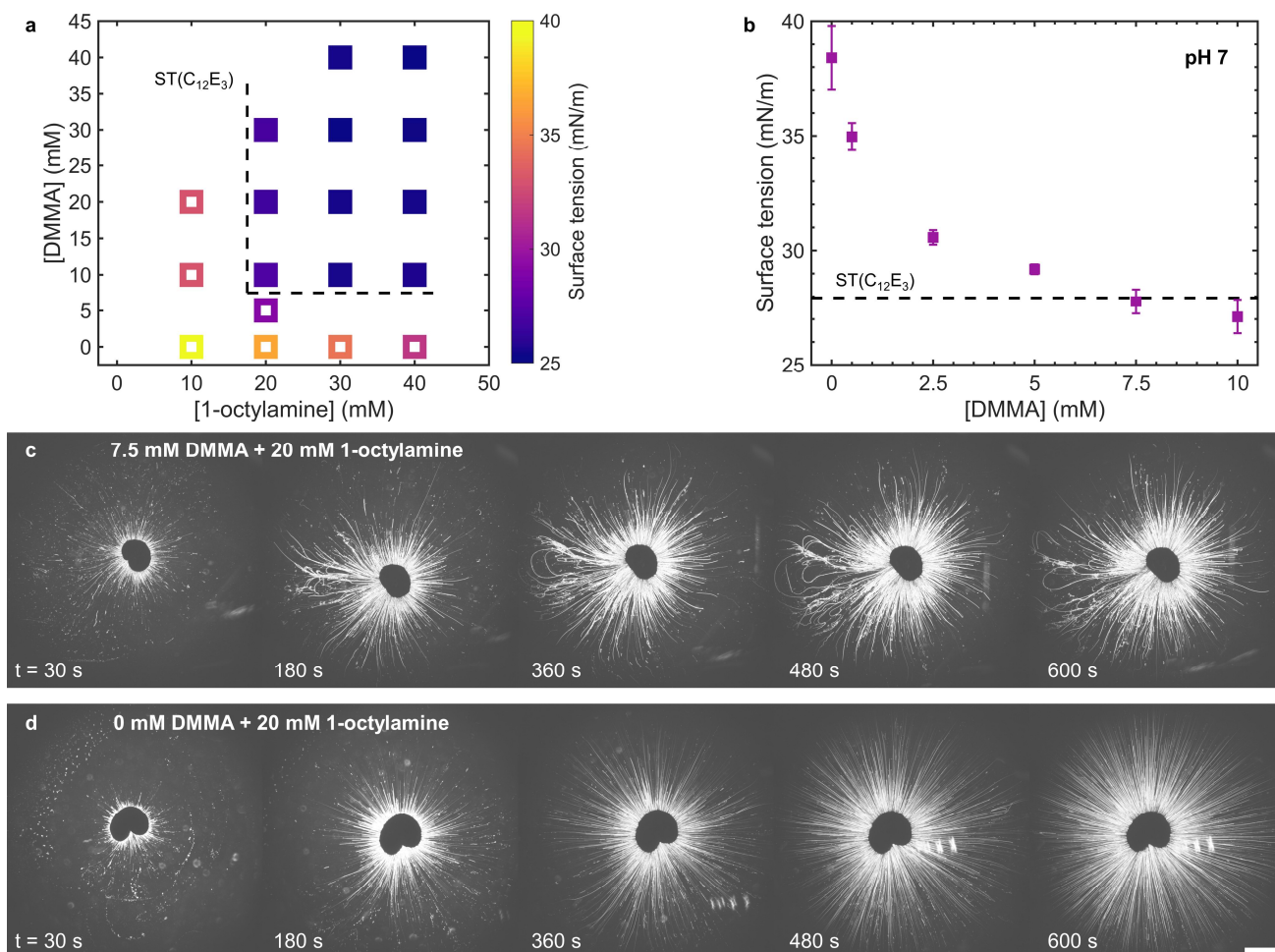


Figure 2. Amide surfactant **2** precursor concentrations required to inhibit $C_{12}E_3$ myelin growth. a) Surface tension at varying concentrations of DMMA and 1-octylamine ($n = 2$). The dashed line indicates the approximate surface tension of $C_{12}E_3$, separating surface tension values higher than that of $C_{12}E_3$ (open symbols) and surface tension values lower than that of $C_{12}E_3$ (closed symbols). b) Average surface tension of amide surfactant **2** at a fixed concentration of 1-octylamine (20 mM) and varying DMMA concentrations. The dashed line indicates the surface tension of $C_{12}E_3$. Error bars display the standard deviation ($n = 3$). c) Optical microscopy recordings of 1 μ L $C_{12}E_3$ deposited on a solution with 20 mM 1-octylamine and 7.5 mM DMMA, showing the inhibition of the myelin growth and the formation of a small myelin corona. d) With a solution of 20 mM 1-octylamine and no DMMA, such that no amide surfactant **2** could be formed, the myelins grow unhampered. The scale bar indicates 2 mm. For all solutions, the pH was set to 7 with a 100 mM sodium phosphate buffer. **[Movie S1]**

Guided by the surface tension measurements, we assessed the capacity of **2** to inhibit the local Marangoni flow generated by a $C_{12}E_3$ droplet at the precursor composition of 20 mM 1-octylamine and 7.5 mM DMMA (in 100 mM PB, pH 7). As shown in Figure 2c and **Movie S1**, the myelins initially grow from the $C_{12}E_3$ droplet (1 μ L), but minutes after deposition of the droplet their growth comes to a halt, so that the myelin corona size stays constant. We note that both the time point at which the myelin growth halts as well as the final corona size varies from droplet to droplet (*vide infra*). Importantly, the myelin growth from a droplet deposited on a 20 mM 1-octylamine solution, in the absence of DMMA, was observed to proceed monotonously (Figure 2d, **Movie S1**). After approximately 6 minutes, the corona fills the entire field of view of the microscope, corresponding to a corona diameter of approx. 14.4 mm. Additionally, for $C_{12}E_3$ droplets deposited on a 7.5 mM DMMA solution, the myelin growth does not halt, although DMMA appears to affect the myelin density in the corona (**Figure S3**, **Movie S1**). Together, our results show that the combination of 20 mM 1-octylamine and 7.5 mM DMMA, at

pH 7, produces sufficient amide surfactant **2** to outcompete $C_{12}E_3$ at the air-water interface, as indicated by the inhibited growth of myelins from the $C_{12}E_3$ droplet.

2.2. Amide surfactant **2** hydrolysis upon addition of acid

Next, we explored the dynamic covalent character of amide surfactant **2** to control the local Marangoni flow generated by $C_{12}E_3$ droplets. The amide surfactant is dynamic covalent due to the proximity of the carboxylic acid to the amide bond (Figure 1c), which makes the amide bond hydrolysable under weakly acidic conditions.^[31,32] Hence, we hypothesized that addition of a small amount of acid hydrolyses the amide surfactant and thereby cancels the inhibition of the myelin growth. Starting off with a 1 μ L $C_{12}E_3$ droplet deposited on an aqueous solution of 20 mM 1-octylamine and 7.5 mM DMMA at pH 7 (100 mM PB), we observe inhibited myelin growth indicating that the local Marangoni flow is suppressed due to the presence of amide surfactant **2** (Figure 3a). Next, addition of HCl (85 μ L, 2 M) results in a rapid increase of the myelin growth after approximately 2 min, resulting in a myelin corona with a radius comparable to experiments in which no amide surfactant **2** was present (Figure 2d). We measured the final pH of the solution to be 6.5.

To assess the hydrolysis dynamics of amide surfactant **2**, we conducted both time-dependent surface tension and quantitative $^1\text{H-NMR}$ measurements. At pH 7.0, we observe a very slow hydrolysis of amide surfactant **2** in $^1\text{H-NMR}$ (Figure 3c), whereas the surface tension stayed constant over a time course of 2 hours (Figure 3b). Upon addition of HCl (2 M) to a solution of DMMA and 1-octylamine in phosphate buffer, to decrease its pH from 7.0 to 6.5, we observe a slow hydrolysis of **2** in $^1\text{H-NMR}$, as well as a slow rise in surface tension over the course of 2 hours. The slow hydrolysis observed at pH 6.5 is in surprising contrast to the fast response in the start of the myelin growth upon the addition of acid displayed in Figure 3a, which led to a pH of 6.5 as well. We hypothesize that the rapid start of myelin growth is caused by imperfect mixing upon the addition of 2 M HCl, resulting in sections of the solution that temporarily have a pH that is much lower than pH 6.5, and thereby facilitate rapid hydrolysis of **2** at low pH. For the $^1\text{H-NMR}$ experiment conducted on the solution of DMMA and 1-octylamine at pH 6.5, we observed a similar phenomenon: compared to the concentration of **2** at pH 7.0, the concentration of **2** already declined by 24% at the start of the $^1\text{H-NMR}$ measurements, approximately 1 minute after addition of 2 M HCl and mixing to end up with a solution at pH 6.5. Gratifyingly, for solutions with DMMA and 1-octylamine at lower pH values (pH 5.5 and 4.0), we observed that right after their preparation – *i.e.* decreasing the pH from 7.0 upon the addition of 2 M HCl – the surface tension approximates the surface tension of 20 mM 1-octylamine at the respective pH value, meaning that all amide surfactant **2** has rapidly hydrolyzed at low pH (Figure 3e).

Together, our results show that we can cancel the inhibitory effect of amide surfactant **2** on the local Marangoni flow and the corresponding myelin growth of $C_{12}E_3$ droplets, by addition of a small amount of concentrated acid to the system. To elicit this response, localized strong decrease of the pH is required to rapidly hydrolyze amide surfactant **2**.

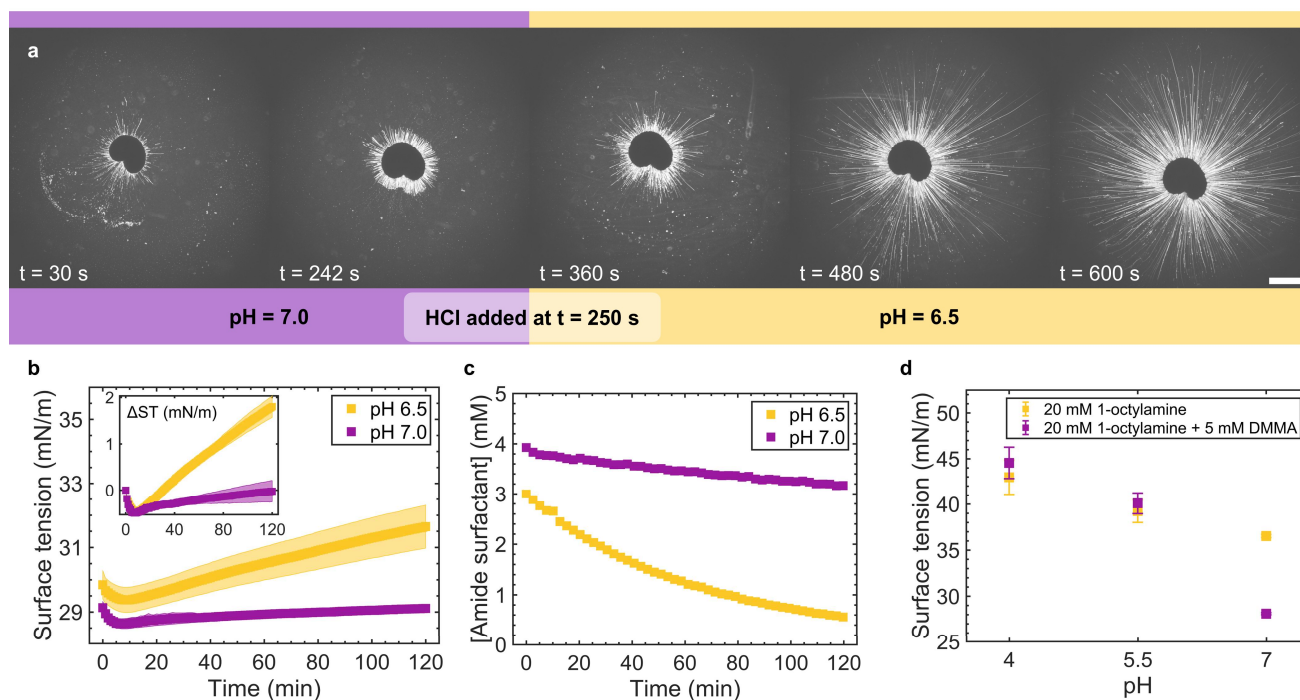


Figure 3. Amide surfactant **2** hydrolyses upon addition of acid. a) Optical microscopy recordings of a 1 μL C_{12}E_3 droplet deposited on a solution with 20 mM 1-octylamine, 7.5 mM DMMA at pH 7 (100 mM PB). At $t = 250$ s, 85 μL 2 M HCl is added to lower the pH to 6.5 and trigger myelin growth. The scale bar indicates 2 mm. b) Time-dependent surface tension, measured on solutions of 20 mM 1-octylamine and 5 mM DMMA at pH 6.5 and 7.0 (100 mM PB). The slow increase in surface tension at pH 6.5 indicates that amide surfactant **2** slowly hydrolyses. The inset shows $\Delta\text{ST} = \text{ST}(t) - \text{ST}(0)$. Error bars indicate standard deviation ($n = 2$). c) Time-dependent concentration of amide surfactant **2**, measured by quantitative $^1\text{H-NMR}$ at pH 6.5 and 7.0 (90:10 100 mM PB: D_2O). At the start of the measurement at pH 6.5, 30% of amide surfactant **2** has been hydrolyzed compared to the measurement at pH 7.0. d) pH-dependent surface tension of 20 mM 1-octylamine and 5 mM DMMA compared to 20 mM 1-octylamine, both at pH 7 (100 mM PB). At pH 4 and 5.5, the surface tension is the same for either solution indicating that no amide surfactant **2** is formed. Error bars indicate standard deviation ($n = 2$).

[Movie S2]

2.3. Multi-droplet deposition using an automated droplet dispenser

To study the self-organization of droplets, as conceptualized in Figure 1e, we developed a droplet dispensing robot that allows for rapid and reproducible deposition of a large number of C_{12}E_3 droplets at the air-water interface. The robot consists of motorized axes mounted to an aluminium base plate to translate a dispensing needle in 3 dimensions (x, y, z) (Figure 4a-b). To dispense C_{12}E_3 droplets, another motorized axis is employed as a syringe pump, connected to the dispensing needle via PTFE tubing. The actions of all motorized axes and syringe pumps can be programmed via a controlling unit that is connected to a computer. The aqueous solution is contained by a circular glass dish (diameter = 131 mm) and supported on top of a circular opening in the base plate. The sample is illuminated by a light source from the bottom, and images of the sample are captured by a camera positioned above the sample (Figure 5b). To deposit C_{12}E_3 droplets precisely at the air-water interface, we use an electrical probing circuit, as described in the Methods section.

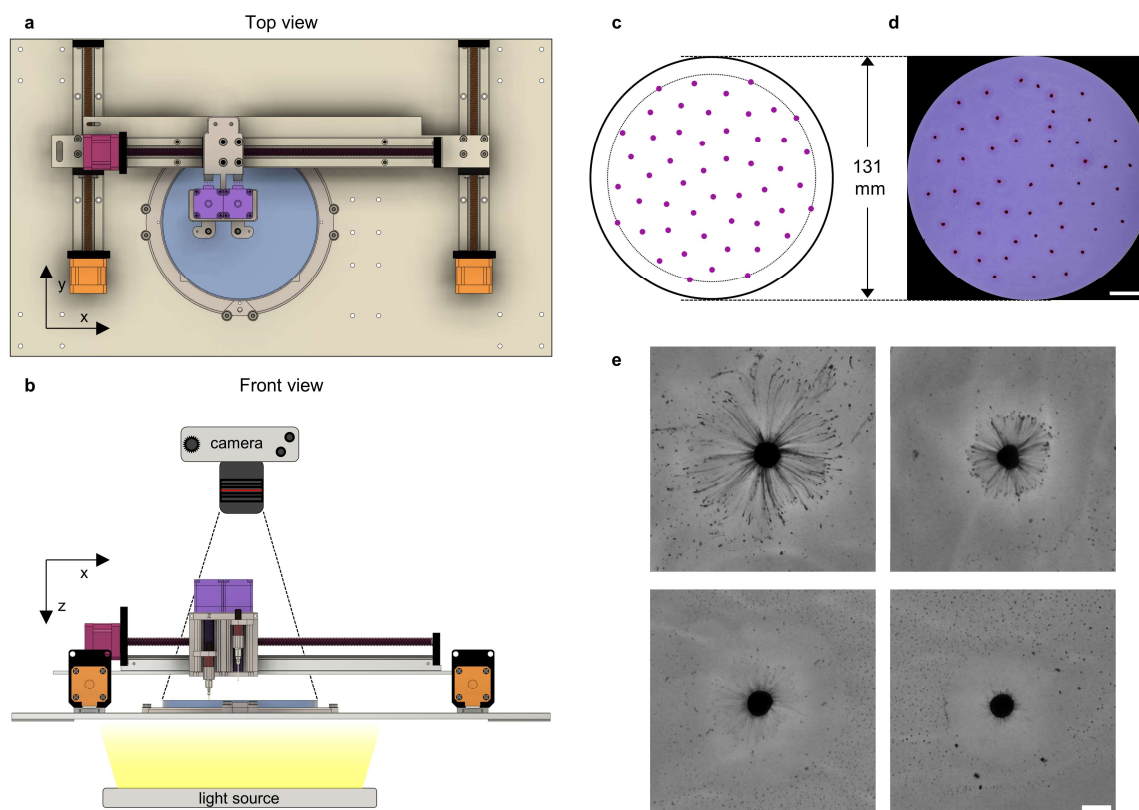


Figure 4. $C_{12}E_3$ droplet deposition with a dispensing robot. a-b) Drawing of the robot setup as seen from the top (a) and front (b). The robot controls the movement of 2 dispensing needles via motorized axes. Two parallel motorized axes (orange) actuate the needles in the y-direction, on top of which a single motorized axis (red) is mounted that actuates the needles in the x-direction. Both dispensing needles are individually actuated in the z-direction by two independent motorized axes (purple). c) Droplet distribution of 50 droplets in the sunflower seed arrangement. The dashed circle indicates the maximum radial position of any droplet $r_{max} = 56.2$ mm that ensures that droplets are not deposited too close to the dish edge. d) Photograph of 50 $1 \mu\text{L}$ $C_{12}E_3$ droplets immediately after deposition on top of a solution of 20 mM 1-octylamine, 7.5 mM DMMA, 0.0025 wt% bromocresol purple at pH 7 (100 mM PB). The scale bar indicates 20 mm. e) Zoomed sections of d) that exemplify variation in the size of the myelin corona. To enhance visibility of the filaments, the blue channel of the RGB image in d) was contrast enhanced. The scale bar indicates 2 mm.

We deposit $1 \mu\text{L}$ $C_{12}E_3$ droplets on a solution of 20 mM 1-octylamine and 7.5 mM DMMA at pH 7 (PB) in the glass dish. To accommodate each droplet with enough space to grow a myelin corona of approx. 1.5-2 mm in diameter, comparable to previously observed myelin corona sizes (Figure 2c, 3a), the area of the glass dish (diameter = 131 mm) provides space for 50 droplets. To ensure that all droplets are homogeneously distributed, we deposit the 50 droplets in the sunflower seed arrangement, in which the angle between neighboring droplets is governed by the golden ratio $\phi = (1 + \sqrt{5})/2$ (Figure 4c). Even though the first few droplets move away from their position, the droplet distribution that is obtained after the deposition process, which takes approx. 8 minutes, is homogeneous and comparable to the sunflower seed arrangement (Figure 4d). The myelin coronas of the deposited droplets vary in size (Figure 4e), but the growth of all myelin coronas halts due to the presence of amide surfactant **2**.

2.4. Spatial differentiation of droplet swarms based on positional information in a pH gradient

We trigger spatial differentiation of the droplets by creating a pH gradient in the aqueous solution. After deposition of 50 $C_{12}E_3$ droplets, we slowly inject HCl (2 M, 1 mL) with the dispensing robot at the bottom of the solution to minimize buoyancy convection due to the higher density of the HCl solution. Control experiments in which NaCl (2 M) instead of HCl was injected, demonstrate that buoyancy convection leads to very slow migration of droplets towards the injection spot, but does not affect myelin growth (**Figure S4** and **Movie S3**). The incorporation of phosphate buffer (100 mM) and the large size of the glass dish ensure that diffusive spreading of the acid is slow. To visualize the resulting pH gradient, we incorporate the pH indicator bromocresol purple in the aqueous solution, which switches color from purple (pH > 6.0) to yellow (pH < 6.0). Immediately after injection of the acid, the pH decreases significantly in an oval-shaped region as indicated by the solution turning yellow (**Figure 5a**).

Immediately after its addition, the acid acts as a chemoattractant to the $C_{12}E_3$ droplets: the droplets in the top area of the dish move rapidly towards the acid and accumulate in the acidic region, as shown in **Figure 5a** ($t = 160$ s) and **Movie S4**. Next, the droplets that have accumulated in the acidic region start to grow longer myelins (**Figure 5b**). Moreover, these droplets become mutually repulsive as indicated by the increase in the droplet-droplet distance inside the acidic region (**Figure 5a**, $t = 600$ s). At the same time, droplets that have not reached the acidic region continue to slowly move in that direction. The combination of this persistent (weak) attraction of the droplets by the acid and the mutually repulsive interactions between droplets that arrive in the acidic region results in a striking droplet configuration: approximately 20 minutes after injection of acid, a droplet wave front emerges at the center of the dish that separates a region of droplets with large myelin coronas from a region of droplets with small myelin coronas. This spatially differentiated myelin growth is clearly revealed in blue-channel, contrast-enhanced images (**Figure 5c**). The self-organized patterns are not equilibrium patterns as can be seen in recordings at $t > 20$ min (**Movie S4**): the pH gradient declines over time and concomitantly, ambient disturbances start to dominate the droplet migration patterns.

The spontaneous organization of the surfactant droplets is a collective effect, i.e. a result of all droplet interactions. Whereas at the start of the experiment, before acid is added, the droplets move rather independently over the interface of the solution, the addition of acid triggers a drastic change in the overall interactions between the droplets. First, the acid hydrolyzes amide surfactant **2**, increasing the surface tension in the acidic region, thereby leading to a global Marangoni flow in the direction of the acidic region (left panel in **Figure 5d**). Second, droplets that arrive to the acidic, surfactant **2**-poor region resume the generation of local Marangoni flow as indicated by the start of myelin growth. These local Marangoni flows push away neighboring droplets, so that few droplets remain in the acidic region. Droplets that have not arrived at the acidic region or droplets that are being repelled by their neighboring droplets closer to the spot where acid was injected, also resume generation of local Marangoni flow, but to a lesser extent: their myelin coronas grow less. Lastly, droplets far away from the acidic region are only attracted by the global Marangoni flow: their myelin coronas do not grow over the time course of the experiment (right panel **Figure 5d**). The self-organization of droplets does not strongly depend on the amount of droplets present in the dish, as indicated by the same pattern formation in control experiments on 25 or 75 $C_{12}E_3$ droplets (**Figure S5**). Taken together, the droplets translate the positional information established by the global pH gradient by differentiating into three morphologically different regions due to the presence of the external pH gradient, analogous to how cells differentiate into ‘French flag’-patterns during morphogenesis.^[33]

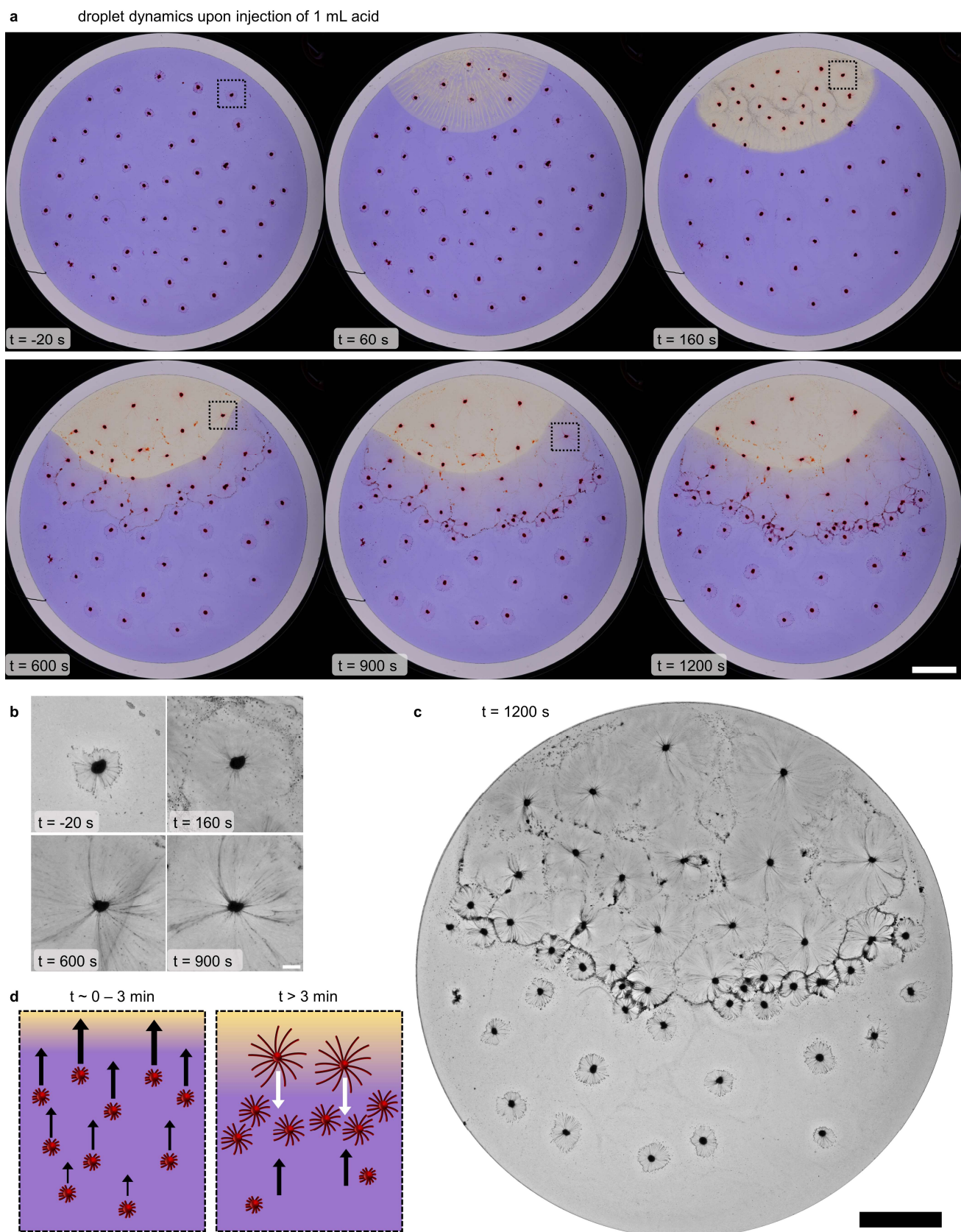


Figure 5. Dynamic self-organization of the droplets into a ‘French flag’-pattern in a pH gradient. a) Photographs of 50 $C_{12}E_3$ (1 μ L) droplets deposited on a solution of 20 mM 1-octylamine, 7.5 mM DMMA, and 0.0025 wt% bromocresol purple at pH 7 (100 mM PB, 35 mL). 1 mL HCl (2 M) is injected into the solution at the top of the dish ($t = 0$). Initially, droplets close to the acid injection spot accumulate in the acidic, yellow region. Subsequently, droplets in the acidic region start to repel each other. Finally, a semicircular region of high droplet density emerges:

a concentrated droplet wave front that separates two regions of low droplet density. The scale bar indicates 20 mm. b) Blue channel, contrast-enhanced sections corresponding to the dashed regions indicated in a). The scale bar indicates 2 mm. c) Blue channel, contrast-enhanced photograph displaying the differences in filament corona size between droplets in the acidic region, the wave front, and the basic region. The scale bar indicates 20 mm. d) Schematic representation of the collective droplet behavior in a pH gradient. Initially, the myelin growth is suppressed due to presence of amide surfactant **2**, and the injected acid (yellow) leads to a global Marangoni flow transporting the droplets towards the acid. Next, local Marangoni flow generated by droplets in the acidic region resumes, as indicated by the increased size of the myelin coronas, and they start to repel neighboring droplets. As a result, most droplets accumulate in a region where the global (black arrows) and local Marangoni flows (white arrows) balance out. [Movie S4]

2.5. Effect of intensity of pH gradient on droplet positioning

To study how the intensity of the pH gradient affects the positioning of the droplet wave front, i.e. the shape of the ‘French flag’-pattern, we varied the amount of acid added to the solution (0.1, 0.5, 1, 2 mL HCl, 2 M). In all experiments, we deposit 50 $C_{12}E_3$ droplets at the surface of the aqueous solution (20 mM 1-octylamine, 7.5 mM DMMA, 0.0025 wt% bromocresol purple, 100 mM PB pH 7). Next, we slowly inject acid ($t = 0$ s), at the same position in the solution and over the same injection time (30 s) for all experiments. As anticipated, both the size of the yellow, acidic region and the number of droplets accumulating in the acidic region increases with increasing amount of acid injected into the solution (**Figure 6a** and **Movies S5-6**). Similarly, the number of droplets that are not significantly affected by the injection of acid, i.e. droplets that keep a constant myelin corona over the duration of the experiment, decreases when more acid is injected (Figure 6b). Importantly, we find that in all experiments, a droplet wave front emerges after approximately 20 minutes, of which the position shifts away from the acid injection spot upon increasing the volume of injected acid.

To quantify how much the droplet wave front shifts upon increasing the amount of acid injected into the solution, we reasoned that the droplets comprising the wave front share 2 quantitative properties: 1) they are close to neighbouring droplets, and 2) they are all positioned approximately at an equal distance away from the spot where acid was injected. To determine the position of the center of the wave front, we first track the (x,y)-position of each droplet with a particle tracking algorithm.^[34] Next, we calculate the distance between each droplet and the position where the acid was injected (R), and we approximate the local droplet density at each droplet position by calculating the nearest neighbour distance for each droplet (d_{NN}), (Figure 6d). Indeed, when we plot the (R, d_{NN})-coordinates for each droplet, the data clusters at low d_{NN} (approx. 7.5 mm) and at R values increasing with increasing amount of injected acid (Figure 6c). Finally, we extract the position of the droplet wave front center \bar{R} by finding the maximum in the (R, d_{NN}) probability density estimate based on all 50 droplet coordinates. When the probability density estimate has more than one maximum, as is the case in the left-most panel in Figure 6c, we select the peak at the lowest d_{NN} value. As shown in Figure 6e, \bar{R} increases with the volume of HCl added, similar to the position of the acid front.

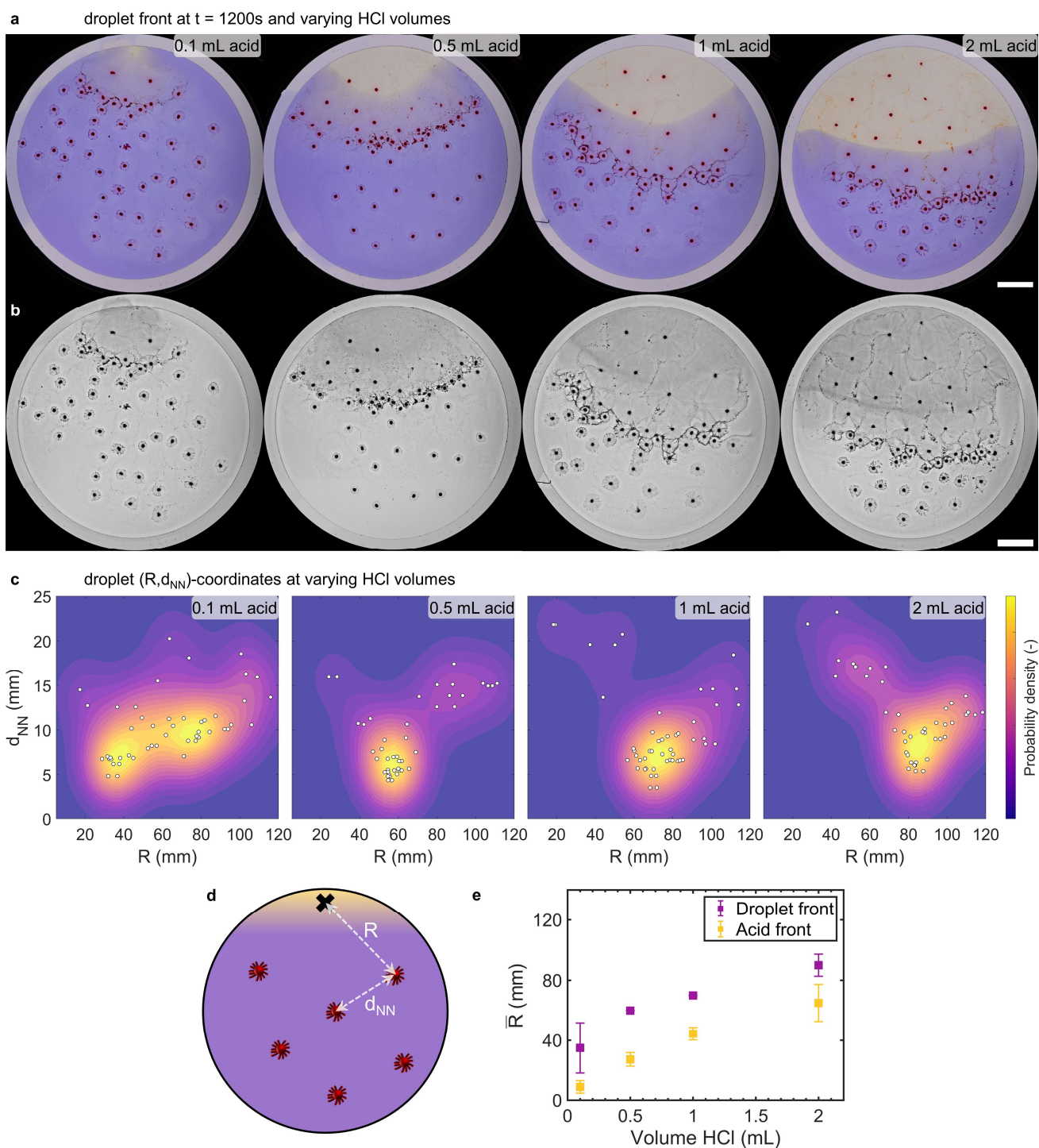


Figure 6. Position of droplet wave front depends on intensity of pH gradient. a) Photographs of 50 $C_{12}E_3$ droplets (1 μ L) deposited on a solution of 20 mM 1-octylamine, 7.5 mM DMMA, and 0.0025 wt% bromocresol purple at pH 7 (100 mM PB, 35 mL), 20 min after varying amounts of HCl (2 M) have been injected into the solution. The scale bar indicates 20 mm. b) Blue channel, contrast-enhanced photographs displaying the differences in myelin corona size between droplets in the acidic region, the wave front, and the basic region. The scale bar indicates 20 mm. c) 2D probability density of droplet coordinates (R, d_{NN}) , see d) at $t = 1200$ s corresponding to experiments in a-b). White datapoints indicate the (R, d_{NN}) coordinates of the 50 $C_{12}E_3$ droplets. d) Schematic representation of (R, d_{NN}) coordinates. R represents the distance of droplet to acid injection spot, d_{NN} the nearest neighbor distance. e) Average position \bar{R} of droplet wave front (purple) and acid front (yellow). Purple \bar{R} values correspond to the R -coordinate of the peaks in the 2D probability density in d). Error bars indicate standard deviation ($n = 3$ separate experiments). [Movie S5, S6]

3. Conclusion

We demonstrate the spatial differentiation of floating $C_{12}E_3$ surfactant droplets into ‘French flag’-patterns based on an external pH gradient. The droplets generate local, mutually repulsive Marangoni flows, visualized by myelin filaments that grow from the droplet periphery, depending on the presence of an amide surfactant that is hydrolyzed under acidic conditions. This competitive amide surfactant adsorbs stronger to the air-water interface than $C_{12}E_3$ and thereby inhibits the local Marangoni flows. When exposed to an external pH gradient, the droplets experience two consecutive effects: 1) a global Marangoni flow arises from the basic side towards the acidic side of the pH gradient, attracting $C_{12}E_3$ droplets towards the acidic side; 2) consecutively, the local Marangoni flows are reestablished by the acid-exposed $C_{12}E_3$ droplets and lead to mutual repulsion between neighboring droplets. This combination of attractive global Marangoni flow and repulsive, position-dependent local Marangoni flows leads to spatial differentiation of the droplet population into three regions of low – high – low droplet density, reminiscent of ‘French flag’-patterns in biological morphogenesis. Furthermore, the morphological difference between the two low droplet density regions is clearly revealed by the difference in myelin growth in either region: long myelins in the acidic region, short myelins in the basic region.

This work demonstrates a strategy to establish morphogenesis in adaptive droplet-based systems. Analogous to how embryonic cells spatially differentiate into patterned tissues based on external “morphogen” gradients,^[33] these surfactant droplets spontaneously differentiate into morphologically distinct regions based on the gradient-induced competition between globally attractive and locally repulsive flows. Marangoni flow offers an attractive design principle to translate a chemical morphogen gradient into motion, due to the direct coupling between surfactant concentration gradient and liquid flow. Moreover, applicability of Marangoni flow is not limited to 2D interfaces, as immersed droplets can be engineered to self-organize based on internal Marangoni flows.^[35,36] Alternative mechanisms in which the driving force responsible for the transport and the transported cargo are susceptible to externally imposed chemical gradients, such as buoyancy convection^[37] or diffusiophoresis^[38] could lead to pattern formations analogous to what we have presented in this work. Droplets are especially attractive as active transport cargos in such a scenario, due to the easy control over their chemical composition and physico-chemical responsiveness. Ultimately, we envision that the concept of competing local and global (Marangoni) flows, combined with droplet swarms that control or self-generate morphogen gradients, allows for adaptation of functional droplet-based materials in response to their environment.

Acknowledgements

We thank W. Huck, D. Karagrigoriou, J. Ferreira, P. Singh, I. Smokers and S. Otto for stimulating discussions. We thank P. White for help with setting up the quantitative NMR experiments. We thank P. Walraven (FNWI Techno Centre Radboud University) for preparing the custom-made glass dishes. The authors thank the Dutch Research Council (NWO, VIDI grant no. VI.Vidi.213.128) as well as the Dutch Ministry of Education, Culture and Science (gravitation program 024.001.035) for financial support.

References

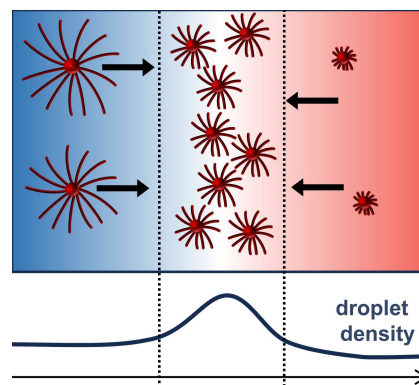
- [1] C. Kaspar, B. J. Ravoo, W. G. van der Wiel, S. V. Wegner, W. H. P. Pernice, *Nature* **2021**, *594*, 345.
- [2] A. Walther, *Adv. Mater.* **2020**, *32*, 1.
- [3] A. Tero, S. Takagi, T. Saigusa, K. Ito, D. P. Bebber, M. D. Fricker, K. Yumiki, R. Kobayashi, T. Nakagaki, *Science* **2010**, *327*, 439.
- [4] M. Le Verge-Serandour, K. Alim, *Annual Review of Condensed Matter Physics* **2024**, *15*, 263.
- [5] L. Tweedy, P. A. Thomason, P. I. Paschke, K. Martin, L. M. Machesky, M. Zagnoni, R. H. Insall, *Science* **2020**, *369*, DOI 10.1126/science.aay9792.
- [6] T. Gregor, K. Fujimoto, N. Masaki, S. Sawai, *Science* **2010**, *328*, 1021.
- [7] M. Skoge, H. Yue, M. Erickstad, A. Bae, H. Levine, A. Groisman, W. F. Loomis, W.-J. Rappel, *Proc. Natl. Acad. Sci. U. S. A.* **2014**, *111*, 14448.
- [8] X. Cheng, J. E. Ferrell Jr, *Science* **2019**, *366*, 631.
- [9] H. Hess, J. L. Ross, *Chem. Soc. Rev.* **2017**, *46*, 5570.
- [10] P. J. de Jong, F. Trigka, M. M. Lerch, *ChemSystemsChem* **2024**, DOI 10.1002/syst.202400005.
- [11] R. Merindol, A. Walther, *Chem. Soc. Rev.* **2017**, *46*, 5588.
- [12] A.-D. C. Nguindjel, P. J. de Visser, M. Winkens, P. A. Korevaar, *Phys. Chem. Chem. Phys.* **2022**, *24*, 23980.
- [13] L. Cera, C. A. Schalley, *Adv. Mater.* **2018**, *30*, e1707029.
- [14] A.-D. C. Nguindjel, P. A. Korevaar, *ChemSystemsChem* **2021**, *3*, e2100021.
- [15] V. Pimienta, C. Antoine, *Curr. Opin. Colloid Interface Sci.* **2014**, *19*, 290.
- [16] C. Jin, C. Krüger, C. C. Maass, *Proc. Natl. Acad. Sci. U. S. A.* **2017**, *114*, 5089.
- [17] I. Lagzi, S. Soh, P. J. Wesson, K. P. Browne, B. A. Grzybowski, *J. Am. Chem. Soc.* **2010**, *132*, 1198.
- [18] S. Soh, K. J. M. Bishop, B. A. Grzybowski, *J. Phys. Chem. B* **2008**, *112*, 10848.
- [19] G. Lu, G. Zhu, Q. Zhang, P. Tian, M. Cheng, F. Shi, *Angew. Chem. Int. Ed Engl.* **2023**, *62*, e202300448.
- [20] J. Čejková, K. Schwarzenberger, K. Eckert, S. Tanaka, *Colloids Surf. A Physicochem. Eng. Asp.* **2019**, *566*, 141.
- [21] B. Kichatov, A. Korshunov, V. Sudakov, V. Gubernov, A. Golubkov, A. Kiverin, *Langmuir* **2021**, *37*, 9892.
- [22] L. Wolpert, *J. Theor. Biol.* **1969**, *25*, 1.
- [23] J. B. A. Green, J. Sharpe, *Development* **2015**, *142*, 1203.
- [24] A. S. Zadorin, Y. Rondelez, G. Gines, V. Dilhas, G. Urtel, A. Zambrano, J.-C. Galas, A. Estevez-Torres, *Nat. Chem.* **2017**, *9*, 990.
- [25] L. Tian, M. Li, A. J. Patil, B. W. Drinkwater, S. Mann, *Nat. Commun.* **2019**, *10*, 3321.
- [26] M. Winkens, P. A. Korevaar, *Langmuir* **2022**, *38*, 10799.
- [27] A. van der Weijden, M. Winkens, S. M. C. Schoenmakers, W. T. S. Huck, P. A. Korevaar, *Nat. Commun.* **2020**, *11*, 4800.
- [28] M. Winkens, A. Vilcan, P. J. de Visser, F. V. de Graaf, P. A. Korevaar, *Small* **2023**, *19*, e2206800.
- [29] A.-D. C. Nguindjel, S. C. M. Franssen, P. A. Korevaar, *J. Am. Chem. Soc.* **2024**, *146*, 6006.
- [30] M. J. Rosen, J. T. Kunjappu, *Surfactants and Interfacial Phenomena*, John Wiley & Sons, **2012**.
- [31] K. Liu, A. W. P. Blokhuis, S. J. Dijt, S. Hamed, A. Kiani, B. M. Matysiak, S. Otto, *ChemRxiv* **2022**, DOI 10.26434/chemrxiv-2022-msgf8.

- [32] S. Su, F. S. Du, Z. C. Li, *Org. Biomol. Chem.* **2017**, *15*, 8384.
- [33] J. Briscoe, S. Small, *Development* **2015**, *142*, 3996.
- [34] J. C. Crocker, D. G. Grier, *J. Colloid Interface Sci.* **1996**, *179*, 298.
- [35] C. H. Meredith, P. G. Moerman, J. Groenewold, Y. J. Chiu, W. K. Kegel, A. van Blaaderen, L. D. Zarzar, *Nat. Chem.* **2020**, *12*, 1136.
- [36] D. Babu, N. Katsonis, F. Lancia, R. Plamont, A. Ryabchun, *Nat Rev Chem* **2022**, *6*, 377.
- [37] S. Maiti, O. E. Shklyaev, A. C. Balazs, A. Sen, *Langmuir* **2019**, *35*, 3724.
- [38] A. Banerjee, T. M. Squires, *Science Advances* **2019**, *5*, eaax1893.
- [39] J. C. Crocker, E. R. Weeks, "Particle tracking using IDL,"
<https://physics.emory.edu/faculty/weeks/idl/>, retrieved at 05/01/2024

Positional information-based morphogenesis of surfactant droplet swarms emerging from competition between local and global Marangoni effects.

Pieter J. de Visser, Mink Neeleman, Pim F. J. Dankloff, Max T. G. M. Derks & Peter A. Korevaar*

Chemical gradients establish positional information and thereby govern cellular differentiation. Analogously, we present surfactant droplets that grow myelin filaments and self-organize in a pH gradient. A competing pH-sensitive surfactant leads to position-dependent myelin growth and droplet-droplet repulsion, because of the emergence of two Marangoni flows: global chemoattraction and local repulsion. As a result, the surfactant droplets organize in ‘French flag’-patterns.



Supporting Information

Positional information-based morphogenesis of surfactant droplet swarms emerging from competition between local and global Marangoni effects.

Pieter J. de Visser, Mink Neeleman, Pim F. J. Dankloff, Max T. G. M. Derks & Peter A. Korevaar*

Table of Contents

Experimental Section

Materials

Methods

Surface Tension Measurements

Microscopy Experiments on Myelin Corona Growth

Quantitative ¹H-NMR measurements to Determine Concentration Amide Surfactant **2**

Description Droplet Dispensing Robot

Deposition Droplet Field

Generation of pH Gradient

Determination of Droplet Positions

Supporting Figures

Figure S1: pH-dependent surface tension measurements of DMMA

Figure S2: ¹H-NMR spectrum of amide surfactant **2**

Figure S3: C₁₂E₃ myelin growth on DMMA solution

Figure S4: NaCl control experiment droplet swarm

Figure S5: Self-organization of 25 and 75 C₁₂E₃ droplets in pH gradient

Description of Supporting Movies S1 – S6

Experimental Section

Materials

Triethylene glycol monododecyl ether ($C_{12}E_3$, > 95%) and 2,3-dimethylmaleic anhydride (DMMA, > 98%) were purchased from TCI Chemicals. Hydrochloric acid (2 M in water), sodium dihydrogen phosphate (99%) and sodium chloride (> 99%) were purchased from Fisher Scientific. Deuterium oxide (99.9%), disodium hydrogen phosphate (> 99%), 1-octylamine (99%), and Oil Red O were purchased from Sigma Aldrich. 3-(Trimethylsilyl)propanoic-2,2,3,3- d_4 acid (TSP- d_4 , > 97.5%) was purchased from Thermo Scientific. 2-propanol was purchased from VWR. All materials were used as received.

Methods

Surface Tension Measurements: Surface tension measurements were performed on a force tensiometer (Biolin Scientific Sigma 701) with a platinum Du Noüy ring (wetting length = 120.4 mm). The ring was cleaned between measurements by rinsing with ethanol and heating with a flame torch until glowing red hot. For each measurement, a Petri dish (Falcon, 35 mm) was filled with 6.0 or 7.0 mL solution. All solutions containing 1-octylamine and/or DMMA were thoroughly vortex-mixed for approx. 30 s and subsequently sonicated for ≥ 20 min until fully dissolved.

Microscopy Experiments on Myelin Corona Growth: Myelin growth of single $C_{12}E_3$ droplets was recorded with an inverted optical microscope (Olympus IX73) equipped with a 1.25x magnification objective (Olympus Plan Apo N 1.25x 0.04 NA). Images were captured in darkfield mode at 1 fps with a CMOS camera (Point Grey Grasshopper3). For each measurement, the lid of a Petri dish (Falcon, 35 mm) was filled with 5.5 mL solution. Next, a $C_{12}E_3$ droplet (1 μ L) was manually pipetted slightly under the surface of the solution to prevent the droplet from bursting. Acid (2 M HCl) is also pipetted under the surface of the solution to limit disturbance of the myelin growth.

Quantitative 1H -NMR measurements to Determine Concentration Amide Surfactant 2: The time-dependent concentration of amide surfactant **2** was measured with 1H -NMR, by calculating the ratio between the peak integrals of the ($C_7H_{15}-CH_2-NH-R$)-protons and that of the ($C_7H_{15}-CH_2-NH_3^+$)-protons of 1-octylamine. We obtain the concentration of amide surfactant **2**, by assuming that the total concentration 1-octylamine and amide surfactant **2** is 20 mM. The samples were prepared from a 90:10 mixture of 22.2 mM 1-octylamine, 5.5 mM DMMA in 100 mM sodium phosphate buffer (pH 7) in H_2O , and 10 mM 3-(trimethylsilyl)propanoic-2,2,3,3- d_4 acid (TSP- d_4) in D_2O . TSP- d_4 was included to indicate 0.00 ppm. A small amount of this solution was used to determine the amount of HCl required to set the pH to 6.5. Next, 1H -NMR measurements were performed for both samples at pH 7.0 and 6.5, using a water peak suppression program (Bruker Avance III, 500 MHz).

Description Droplet Dispensing Robot: The droplet dispensing robot (developed by Labm8) comprises 7 motorized axes that are controlled by a controlling unit (Labm8, M8001.1). $C_{12}E_3$ and HCl solution were dispensed from 2 blunt, stainless-steel needles (Fisnar, inner diameter: 0.8 mm; 21 Ga). The position of the dispensing needles was independently actuated by 2 motorized axes in z, 1 motorized axis in x, and 2 parallel motorized axes in y (Figure 4a-b). The $C_{12}E_3$ dispensing needle was connected to a glass syringe (Hamilton, 1.5 mL) and the HCl solution dispensing needle to a glass syringe (Hamilton, 25 mL) with PTFE tubing. The syringes were actuated by motorized axes, i.e. syringe pumps (Labm8, M8003.1). All motors were calibrated stepper motors, so that the imposed actuation in steps can be converted to movement in millimeters or volume in microliters. The motorized axes were mounted onto an aluminum base plate. The entire setup was mounted on an anti-vibration optical table and levelled using adjustable legs.

To enhance the visual contrast between $C_{12}E_3$ droplets and the aqueous solution in recorded images, the dye Oil Red O (20 mg/mL) is incorporated into the surfactant solution. To deposit $C_{12}E_3$ droplets precisely at the air-water interface, we used a 2 wire analog electrical probing circuit connected to the stainless-steel needle that dispensed the droplets and a copper wire positioned inside the aqueous solution. When the needle and the surface of the aqueous solution come into contact, a signal is registered (above a set threshold), which is interpreted by the robot to stop motion in the z-direction after which it starts dispensing $C_{12}E_3$. In all our experiments, we used solutions containing 100 mM sodium phosphate buffer, which was sufficient for the probe to detect an over-threshold event. Droplets were deposited on a solution contained in a thin, custom-made glass dish (inner diameter: 131 mm, thickness: 2 mm) held in place over a circular hole in the base plate.

The sample was illuminated with a LED panel (Viltrox VL-200T, color temperature 5600 K) and was diffused with a thin (3 mm) sheet of frosted polymethyl methacrylate. Images were captured with a mirrorless camera (Nikon Z5) and macro lens (Laowa 100 mm f/2.8). For all experiments the camera settings were as follows, ISO: 100, shutter speed: 1/25 s, aperture: f22, white balance: daylight, capture rate: 1 frame every 20 seconds.

Deposition Droplet Field: $C_{12}E_3$ droplets were deposited in the sunflower seed arrangement to ensure homogeneous spreading in the circular dish. We computed the position of droplet i in polar coordinates (r_i, θ_i) with (0,0) at the center of the dish as

$$r_i = r_{max} \cdot (\sqrt{i - 1/2} / \sqrt{(n - b + 1)/2}) \quad (1)$$

$$\theta_i = 2\pi i / (\phi - 1) \quad (2)$$

with $r_{max} = 56.2$ mm the radius of the deposition zone, n the total number of droplets, $b = 7$ the number of droplets on the boundary of the deposition zone, and ϕ the golden ratio $(1 + \sqrt{5})/2$. We chose r_{max} so that droplets are not deposited closer to the edge of the dish than 0.5 times the average droplet-droplet distance, i.e. $r_{di} - r_{max} = \sqrt{A_{dish}/(n \cdot \pi)}$, where A_{dish}/n is the average area per droplet. The droplet coordinates were computed, converted to robot coordinates, and exported to a G-code file. The G-code file also includes the dispensing flow rate and needle movement rate (x,y: 500 mm min⁻¹, z: 100 mm min⁻¹). The dispensing flow duration for $C_{12}E_3$ was set to 2 s (0.5 $\mu\text{L s}^{-1}$), the dispensing flow duration of HCl solution was set to 30 s for all volumes of dispensed HCl solution.

Generation of pH Gradient: To generate a pH gradient, a HCl solution (2 M) was injected with the droplet dispensing robot into the aqueous solution at a fixed position in the dish, approx. 1 mm offset from the edge of the dish. To minimize buoyancy convection due to the density difference of the HCl solution ($\rho = 1.04 \pm 0.00$ g mL⁻¹) and that of the aqueous solution ($\rho = 1.01 \pm 0.01$ g mL⁻¹, 7.5 mM DMMA, 20 mM 1-octylamine, 100 mM PB pH 7, 0.0025 wt% bromocresol purple), the HCl solution was injected at the bottom of the solution, approx. 0.5 mm above the bottom of the dish. Both solution densities were measured by weighing known volumes of these solutions ($n = 10$).

Determination of Droplet Positions: To determine the droplet positions based on the recorded timelapse frames, we used the MATLAB implementation of a particle tracking algorithm originally developed by Crocker and Grier.^[34,39] Here, we will give a comprehensive overview of the analysis steps with algorithm and MATLAB function names in italics.

Step 1 - Pre-processing: First, we removed parts of the original frames outside the dish, including the dish edges, by binarizing the frames (*imbinarize*) and cropping the regions of intensity 0 (*imcrop*). Second, we discarded the red and green channels from the RGB frames as the red $C_{12}E_3$ droplets contrast most against the background in the blue channel. Next, we inverted the color scale of the resulting frame (*imcomplement*) so that the droplets appear bright against a dark background. Lastly, we resized the image to 1/9th the original size (*imresize*) to speed up computation.

Step 2 - Droplet tracking: The pre-processed frames were sequentially filtered using a bandpass filter (*bpass*) with high frequency cutoff set to 11 pixels and low frequency cutoff set to 21 pixels. Next, droplet positions in each frame were identified (*findfeatures*) based on the size (35 pixels) and minimum pixel brightness (5) of bright spots in the filtered frames. Finally, the identified spots were evaluated and another filter was applied (spot brightness > 3500, spot size < 120 pixels, spot eccentricity < 0.15).

Step 3 - Computation of droplet coordinates R and d_{NN} and probability density estimation: Droplet coordinates in x,y were converted to coordinates $R = ((x_i - x_{acid})^2 + (y_i - y_{acid})^2)^{1/2}$, i.e. the distance between droplet i and the acid injection spot, and the nearest neighbor distance $d_{NN} = \min[((x_i - x_j)^2 + (y_i - y_j)^2)^{1/2}]$. Subsequently, the droplet probability density was estimated using a 2D kernel estimator (*mvksdensity*) with bandwidth 10 and 3 in R and d_{NN} respectively. Finally, the probability densities were plotted in a filled contour plot (*contourf*).

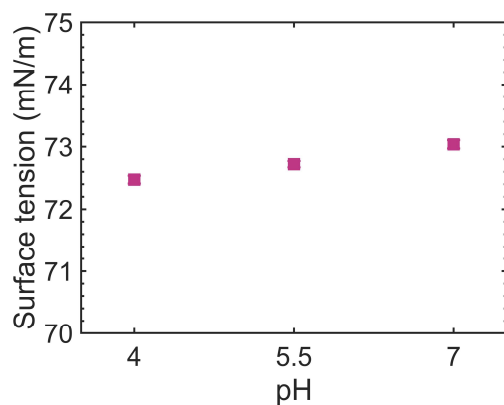


Figure S1. pH-dependent surface tension measurements of 5 mM DMMA in water ($n = 2$). The error bars are smaller than data indicators due to the low standard deviation between measurement data.

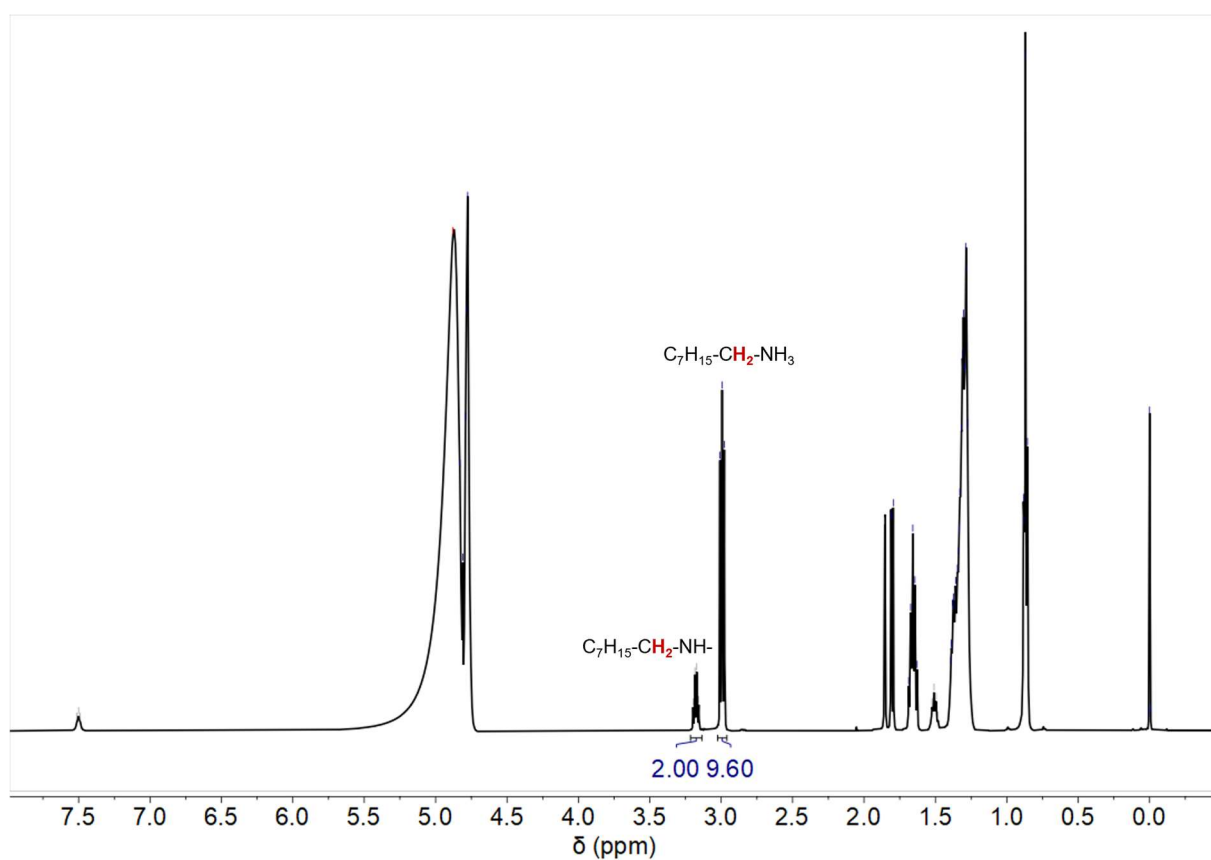


Figure S2. 1H -NMR spectrum of 5 mM DMMA, 20 mM 1-octylamine in 100 mM PB pH 7 in a 90:10 $H_2O:D_2O$ solution, with TSP- d_4 (1 mM). The protons neighboring the amine group of 1-octylamine at 3.0 ppm and the corresponding protons of amide surfactant **2** at 3.2 ppm are indicated in red.

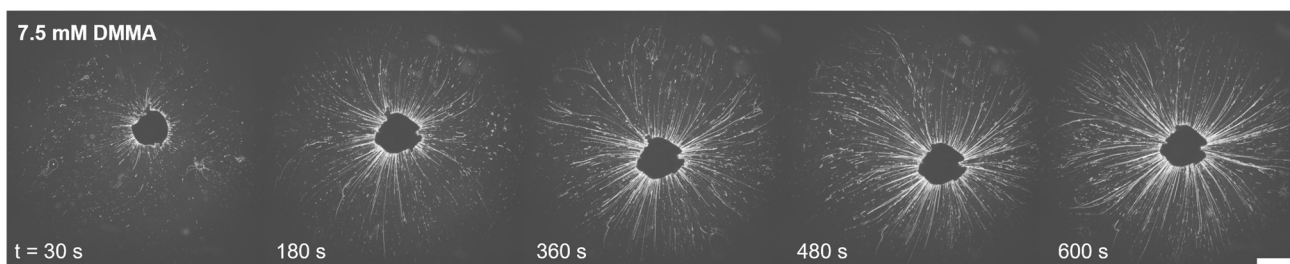


Figure S3. Optical microscopy recordings of 1 μL C_{12}E_3 deposited on a solution with 7.5 mM DMMA at pH 7 (100 mM PB). Myelin growth is slightly hampered by DMMA, although the growth does not halt as compared when 1-octylamine is incorporated in the solution (cf. Figure 2c). The scale bar indicates 2 mm.

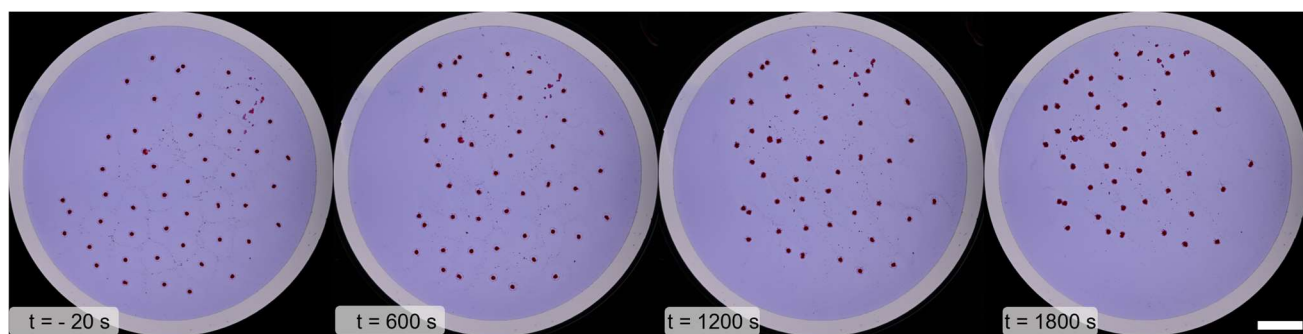
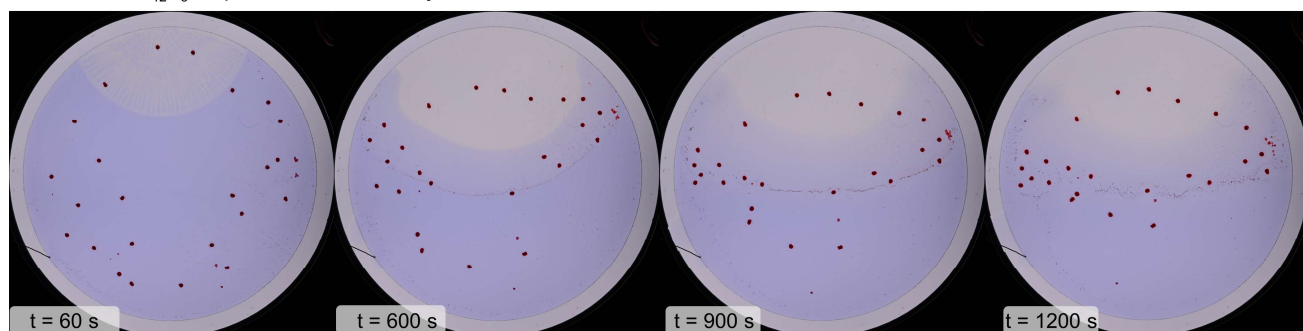


Figure S4. Photographs of 50 C_{12}E_3 droplets (1 μL) deposited on a solution of 20 mM 1-octylamine, 7.5 mM DMMA, and 0.0025 wt% bromocresol purple at pH 7 (100 mM PB, 35 mL). At $t = 0$ s, 1 mL NaCl (2 M) was injected with the droplet dispensing robot at the top of the dish. No myelin growth is observed. There is a small drift of the droplets towards the spot where salt was injected. The scale bar indicates 20 mm.

a 25 C_{12}E_3 droplets; 1 mL 2 M HCl injected



b 75 C_{12}E_3 droplets; 1 mL 2 M HCl injected

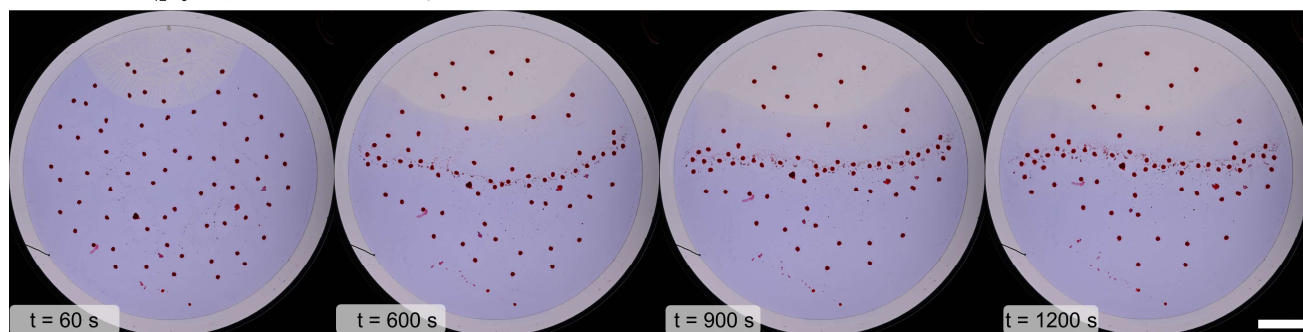


Figure S5. Photographs of 25 (in a) and 75 (in b) C_{12}E_3 droplets (1 μL) deposited on a solution of 20 mM 1-octylamine, 7.5 mM DMMA, and 0.0025 wt% bromocresol purple at pH 7 (100 mM PB, 35 mL). The scale bar indicates 20 mm.

Description of Supporting Movies S1 – S6

NB. Time is indicated in (HH:)MM:SS format in all Supporting Movies.

File Name: Movie S1 – Optical microscopy recording corresponding to Figures 2c-d and S3

C₁₂E₃ myelin growth on aqueous solutions with amide surfactant **2** (left panel), with precursor 1-octylamine (middle panel), or with precursor DMMA (right panel). Myelin growth only fully halts if amide surfactant **2** is present. DMMA destabilizes the myelins, but myelins continue to grow. All solutions are set to pH 7 (100 mM PB).

File Name: Movie S2 – Optical microscopy recording corresponding to Figure 3a

Reactivation of C₁₂E₃ myelin growth on an aqueous solution with amide surfactant **2** (7.5 mM DMMA, 20 mM 1-octylamine) upon addition of HCl solution at t = 250 s. Initially, the pH of the solution is set to pH 7 (100 mM PB), and after addition of HCl the pH is measured to be 6.5.

File Name: Movie S3 – Time lapse recording corresponding to Figure S4

Control experiment for droplet swarm self-organization. NaCl (2 M, 1 mL) was injected into the solution instead of HCl at t = 0 s. Over the course of approx. 30 minutes myelins do not grow, but the droplets slowly drift towards the spot where NaCl was injected, and some droplets clump together.

File Name: Movie S4 – Time lapse recordings corresponding to Figure 5a

Full color (RGB, left) and contrast enhanced, blue channel (right) recordings of the self-organization of 50 C₁₂E₃ droplets in a pH gradient. The aqueous solution contains 7.5 mM DMMA, 20 mM 1-octylamine, 0.0025 wt% bromocresol purple and is set to pH 7 (100 mM PB). At t = 0 s, 1 mL HCl (2 M) is injected into the solution with the droplet dispensing robot. The ‘French flag’-pattern is established approx. 20 minutes after addition of the acid.

File Name: Movie S5 – Time lapse recordings corresponding to Figures 6a-b

Full color (RGB, top row) and contrast enhanced, blue channel (bottom row) recordings of the self-organization of 50 C₁₂E₃ droplets in a pH gradient. The aqueous solution contains 7.5 mM DMMA, 20 mM 1-octylamine, 0.0025 wt% bromocresol purple and is set to pH 7 (100 mM PB). At t = 0, the indicated amount of HCl (2 M) is injected into the solution with the droplet dispensing robot.

File Name: Movie S6 – Time lapse recordings corresponding to Figure 6e

Full color (RGB) recordings of the self-organization of 50 C₁₂E₃ droplets in pH gradients of different intensities (0.1, 0.5, 1, 2 mL HCl solution added). The aqueous solution contains 7.5 mM DMMA, 20 mM 1-octylamine, 0.0025 wt% bromocresol purple and is set to pH 7 (100 mM PB). At t = 0, the indicated amount of HCl (2 M) is injected into the solution with the droplet dispensing robot.